Eur. Phys. J. B **46**, 457–461 (2005)
DOI: 10.1140/epjb/e2005-00274-4

THE EUROPEAN PHYSICAL JOURNAL B

Si/SiO_2 core shell clusters probed by Raman spectroscopy

G. Faraci[1,a], S. Gibilisco[1], P. Russo[1], A.R. Pennisi[1], G. Compagnini[2], S. Battiato[2], R. Puglisi[3], and S. La Rosa[4]

[1] Dipartimento di Fisica e Astronomia, Università di Catania; MATIS - Istituto Nazionale di Fisica della Materia, Via Santa Sofia 64, 95123 Catania, Italy
[2] Dipartimento di Scienze Chimiche, Università di Catania; MATIS - Istituto Nazionale di Fisica della Materia, Viale Andrea Doria 6, 95123 Catania, Italy
[3] IMM, Consiglio Nazionale delle Ricerche, Catania, Italy
[4] Elettra, Sincrotrone Trieste, Trieste, Italy

Received 23 February 2005 / Received in final form 23 May 2005
Published online 7 September 2005 –

Abstract. Using a pulsed microplasma source, clusters were produced through the ablation of a Si cathode and successive supersonic expansion. The Si cluster beam was deposited onto different substrates and the partial oxidation of the cluster surface avoided the growth of large agglomerates, preserving their nanocrystalline morphology. Micro-Raman spectroscopy was used for an accurate size diagnosis of the deposited nanoparticles. The size of the Si dots ranges between 2 and about 15 nm. The Si dots appear to have a Si oxide shell, as confirmed also by structural and compositional analysis through transmission electron microscopy and atomic force microscopy. Double Raman peaks were attributed to small Si agglomerates having a thin substoichiometric Si-O interface.

PACS. 36.20.Ng Vibrational and rotational structure, infrared and Raman spectra – 36.40.Mr Spectroscopy and geometrical structure of clusters – 61.46.+w Nanoscale materials: clusters, nanoparticles, nanotubes, and nanocrystals – 81.07.Ta Quantum dots

The synthesis of size selected Si nanocrystals represents a wide field of important research. They are of great interest not only from a fundamental point of view [1–8] but also for their applications in optoelectronics and device technology [9–11]. Several methods are used for Si nanocrystal or quantum dot production, including plasma enhanced chemical vapor deposition [6], pulsed cluster beams [5], laser induced decomposition of SiH_4 in a gas flow reactor [2,3], and ion implantation [9].

For practical use, the nanocrystals should ideally have a narrow size dispersion, since the quantum confinement effects are size dependent; therefore, they should be deposited on or embedded in a suitable matrix, avoiding their coalescence or the growth of a thick layer. A narrow size dispersion can easily be achieved using a mechanical selection with a time of flight chopper in cluster beams [1], whereas cluster coalescence could in principle be prevented by coating the individual clusters with a protecting thin layer. This is not an easy task, although several experiments have confirmed that, under proper conditions, clusters can preserve their morphology while deposited on a substrate [2].

We are particularly interested in the synthesis of Si quantum dots, in a size range of a few nm, since, at this size, optical transitions forbidden in the bulk can be obtained in the nanocrystals. In this range, however, quantum dots can mutually interact on the matrix, forming larger agglomerates which increase the spread of the size distribution. Characterization of Si quantum dots often gives conflicting results: Raman results [6,8,12] not only exhibit a wide spread but also do not agree with the theoretical calculations; [4,8] on the other hand, for photoluminescence measurements [1,3] in some cases, good agreement between experiment and theory is reported.

Our cluster production is performed by a microplasma source usually working in ultra high vacuum [11,13]. The microplasma is produced by a spark discharge between two B doped Si electrodes in He atmosphere. Ultrapure He carrier gas enters the source, at $p = 10$ bar, through a pulsed valve. The gas, ionized by the discharge, acts as an ion gun eroding the Si cathode. Supersonic expansion of Si-seeded He gas in a second vacuum chamber through nozzle and skimmers allows the deposition of the cluster beam on a metal substrate. Simply modifying the base pressure, and working with a low oxygen exposure in the main chamber, permitted the formation of an external Si dioxide layer on the cluster surface. This simple expedient avoided cluster coalescence, maintaining the initial size and shape characteristics during the sample deposition [12]. The external coating layer can also be quite

[a] e-mail: Giuseppe.Faraci@ct.infn.it

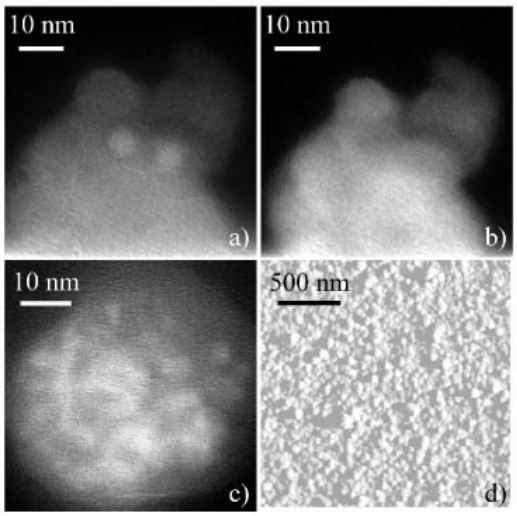

Fig. 1. (a) Typical EFTEM (by a JEOL 2010F TEM equipped with a energy filtering system) micrograph in plan view obtained on the Si nanocrystals, with energy selected bright field imaging tuned to 16 eV (typical of Si plasmon loss); (b) with energy selected at 26 eV (SiO_2 plasmon loss), showing the Si oxide surrounding the Si dots; (c) with energy selected at 16 eV, showing a large group of Si dots; (d) typical AFM micrograph showing that the Si dots are uniformly distributed on the substrate.

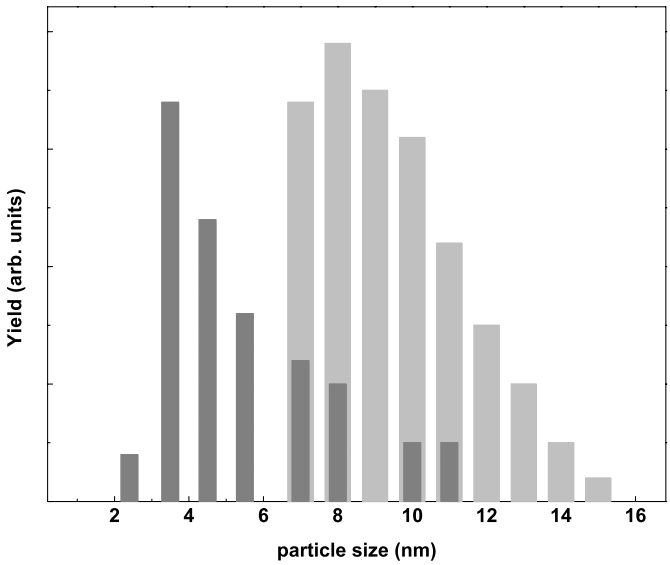

Fig. 2. Cluster size distribution evaluated by analyzing the EFTEM and Raman spectra in the range 2–12 nm (left histogram) and AFM images in the range 6–17 nm (right histogram) on different regions of the substrate. The low size limit for AFM is due to tip resolution. Typical uncertainty is of the order of 20%. Note that the two histograms collected by different sampling methods have different arbitrary scales.

useful for semiconductor passivation, when technological applications are considered.

In addition, the adopted method allowed the accumulation of several layers of clusters with a nanocrystal semiconductor core separated by an insulating layer of oxide. This high concentration was extremely useful for optical characterization performed by micro-Raman spectroscopy.

The cluster beam after the skimmer is spread radially according to the cluster size; this allowed us to collect the entire ensemble of clusters on the same substrate, obtaining different sizes in different positions about 100 μm distant from each other.

Several samples were obtained on different substrates (metals, pyrolitic graphite) chosen ad hoc according to the particular spectroscopy used for their characterization. The size and the size dispersion of our samples were checked by Energy Filtering Trasmission Electron Microscopy (EFTEM) and Atomic Force Microscopy (AFM), and compositional information was given by electron energy loss spectroscopy. Experimental details can be found in reference [13]; the Si dots, represented in Figure 1a by the circular white isolated spots with a radius of about 2 nm, are surrounded by a shell of SiO_2, of about 4 nm in thickness, as confirmed by compositional analysis through EFTEM (Fig. 1b). Figure 1c shows a larger group of Si dots. AFM analyses, shown in Figure 1d as an example, and performed all over the deposited film, demonstrate the uniformity of the layer, on the AFM scale (500 nm); examination of the entire sample allows us to obtain the size distribution on a particular substrate.

In Figure 2 the size distribution of the deposited agglomerates is displayed in two histograms.

The first, on the right hand side, shows the size dispersion evaluated ex situ by AFM in the range 6–17 nm; this technique gives the global size of the deposited clusters, composed of an internal Si crystal core surrounded by an oxide layer of substoichiometric configuration at the interface with the Si core.

The second histogram, on the left side, is obtained by Raman and Si-Energy-Filtered-TEM, both sensitive only to Si nanocrystals; in fact, this size distribution is shifted to lower sizes (2–12 nm) and this suggests the average thickness of the oxide shell is about 2.5 ± 0.5 nm. This implies that the Si nanocrystals smaller than 2 nm in the initial stage can be completely oxidized.

For optical micro Raman analyses, the Si quantum dots were deposited on a Cu thin foil since the substrate does not exhibit any contribution in the frequency range of our samples. The Raman spectrometer was equipped with an Ar ion laser; 514.5 nm (2.4 eV) and 457.9 nm (2.7 eV) radiation was used as exciting photon source. Laser power was always maintained below 20 mW to minimize heating effects on the focused spot (size of about 5 μm).

As well known in the literature, the resonant Raman spectrum for crystalline c-Si(111) performed with excitation wavelength 363.8 nm (3.34 eV) gives a resonant peak at 520 cm^{-1}; this corresponds to the allowed phonon excitation at $k \approx 0$ [3,4]. Similar results have been obtained for c-Si by Ehbrect et al. [3] and Guyot et al. [14] with a non-resonant light of longer excitation wavelength [514.5 nm (2.4 eV)], observing the Raman signal at $\omega = 521$ cm^{-1}.

First, we display in Figure 3 the micro Raman reference spectrum for the B-doped bulk Si electrode used as

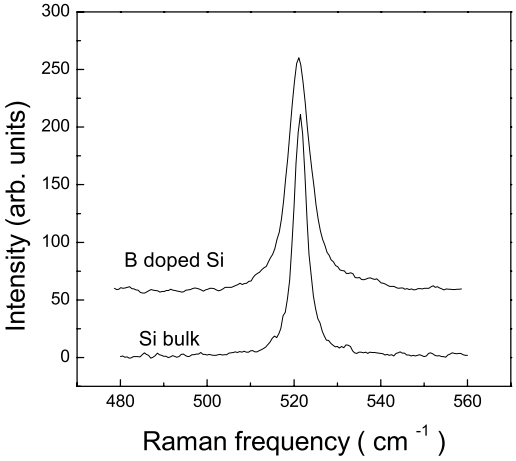

Fig. 3. Micro Raman reference spectrum for our B doped Si cathode, with respect to a pure bulk Si substrate. Clearly visible is the larger linewidth (5.1 cm^{-1}) of the doped semiconductor, whereas pure Si exhibits a width of 3.0 cm^{-1}. A minor shift of 0.4 cm^{-1} is also detected.

a cathode in our plasma source. We observe a peak at the position $\omega = 521.1$ cm^{-1} with a full width at half maximum $\Delta w = 5.1$ cm^{-1}. This value can be compared with an intrinsic (single crystal) Si spectrum giving respectively $\omega = 521.5$ cm^{-1} and $\Delta w = 3.0$ cm^{-1}.

This weak modification can be attributed to the heavy doping (3×10^{18} atoms/cm^3) of the semiconductor by means of boron impurities.

In Figure 4 we show some typical micro Raman spectra obtained for our Si QD's with different size, as checked by EFTEM.

We note contributions giving size dependent Raman shifts $\Delta\omega$, with different peak broadening Δw. In the same figure, we report the deconvolution of each spectrum, showing in several cases the superposition of two overlapping features. This result is particularly important for the following reasons:

(i) it is the first experimental observation of such an overlap with Raman features well separated; in fact, in the past only mathematical deconvolutions [6] were suggesting more than one component;
(ii) these double structures exhibit a relative intensity quite different with respect to each other and this is extremely challenging for the interpretation, as discussed later;
(iii) the linewidth of each feature can be extracted without any mathematical multiparameter fitting procedure, avoiding any possible ambiguity.

Let us now present the analysis of the present Raman data, comparing with similar results. As reference we use the few experimental spectra reported in the literature [2,6,8] for Si clusters with size in the nanometer range. These show a large shift due to the quantum confinement effects reported as a function of the nanocrystal size in Figure 5a. Although a large uncertainty is visible, the trend of the data can be assumed as a rough reference and used as a calibration. With this assumption, in

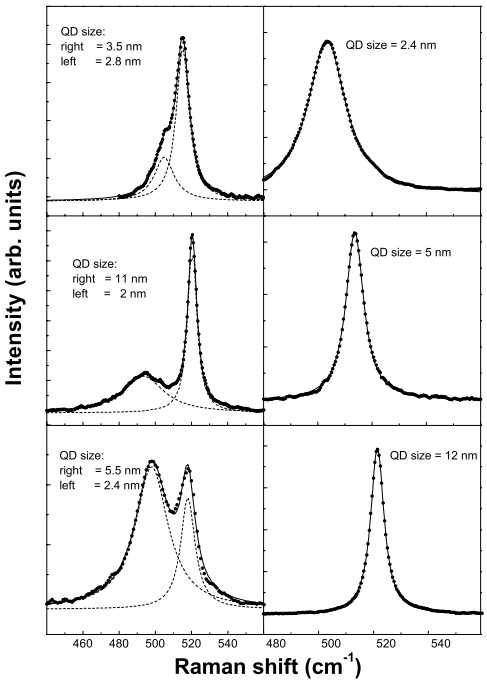

Fig. 4. Typical micro Raman spectra obtained for our Si QDs. On the left column double components unambiguously indicate the presence of two well resolved contributions. Lorentzian lineshape was used for fitting each feature with an excellent overall agreement with the experimental data. Similarly for single components on the right column. The size indicated in each figure is extracted from the Raman plot (see text). Note the different position and width of each curve.

Figure 5b we report our data, observing that the size obtained by EFTEM for our nanocrystal dots are in qualitative agreement with those deduced from the Figure 5a.

As already mentioned, a further check was performed on the samples by atomic force microscopy: as visible in Figure 1, the size distribution of our QD was quite uniform and relatively narrow. In addition, we can show the plot of the correlation between the Raman full width at half maximum and the Raman shift already mentioned. We observe a quasi linear increase of the linewidth as the shift increases or, in other words, when the size is reduced (see Fig. 5c).

These experimental observations can also be compared with theoretical models of Richter et al. (RWL, Ref. [12]) and the Bond Polarization Model (BPM, Ref. [8]) (see Fig. 5); these models take into account the quantum confinement effects due to the very small size of the quantum dots; both can be presented in the form

$$\Delta\omega = -\alpha(a/d)^{\gamma}$$

where a is the lattice parameter (for Si $a = 0.543$ nm), d is the cluster diameter, whereas α and γ are the following parameters:

(i) for the Richter model $\alpha = 52.3$ cm^{-1} and $\gamma = 1.586$;
(ii) for the bond polarization model $\alpha = 47.41$ cm^{-1} and $\gamma = 1.44$.

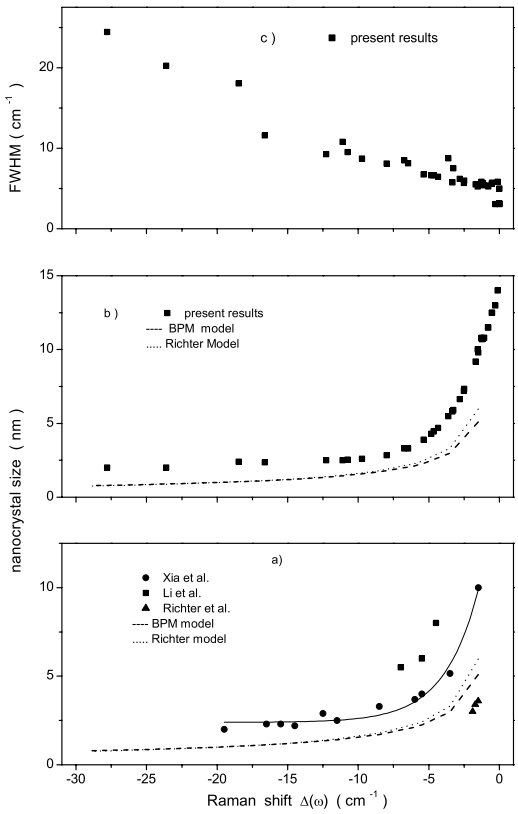

Fig. 5. (a) Si nanocrystal size vs. Raman shift from literature data, the line connecting the Xia et al. points is a best fit of these data. Also reported are two theoretical models; the agreement with experiment is quite poor. (b) Our Raman results plotted using as reference the fitting line of Xia et al. data. Uncertainty for the nanocrystal size is of the order of 10% resulting from the size spread of the dispersion curves. Also shown are the theoretical models. (c) Full width at half maximum of the Raman peaks of our spectra plotted against the corresponding Raman shift. The trend is quasi-linear.

As discussed in reference [8], a strong correlation can be experimentally observed between the Raman peak position, its linewidth and the size of the nanocrystals. However, the theoretical models cannot reproduce these features and should be refined taking into account further effects such as the size related strain modifications [6].

Furthermore, recently [15], useful calculations have been performed in order to evaluate the spectral relative intensity of each feature, taking into account not only optical modes but also low energy acoustical modes. In any case, at present the agreement is only qualitative, as reported in Figure 5, where the experimental data are presented together with the theoretical models.

We discuss now in some detail our results, emphasizing the wide range of Raman shifts covered by our measurements. The method we adopted for the quantum dots synthesis has produced many different agglomerates separated on the substrate without significant coalescence, and allows the detection of a single Raman peak somewhat broadened by two concomitant effects; the first is due to the size spread, the second one to the size confinement, i.e., to the low dimension of the QDs. The size spread of course produces the superposition of several components shifted as a function of the size, and therefore causes a line broadening. The size confinement, even in ideal nanocrystals of a single size, produces a lack of crystal periodicity and therefore the confined phonon is coupled to each Raman phonon branch whose dispersion $\omega(\mathbf{q})$ is highly anisotropic in Si [16].

We emphasize that the poor agreement between the experimental data and the theoretical calculations (see Fig. 5) could be ascribed to the partial description of the phonon modes, often limited to the optical branches and neglecting the acoustical ones [15,17].

In several cases, as shown above, two well resolved components were detected in our experiments. This can be attributed to the possible presence of a dual or binary size distribution, for which two different sizes are preferentially formed. This was observed for Kr clusters at low temperature by Andersen et al. [18]. As these double features do not seem to be associated to correlated sizes, the high intensity and the shape indicate that they originate from nanocrystals. In fact, we did not observe any possible dynamic effect (such as, e.g., crystallization of amorphous components under the laser beam). Neither can these features be ascribed to the B doping of the Si electrodes, since the relative impurity concentration is lower than 10^{-4}, and its effect, as shown in Figure 2, is limited to a negligible shift and broadening. Other hypotheses however are under investigation. An alternative explanation may be that suggested by Xia et al. [6] hypothesizing a central crystalline core of the quantum Si dot and a surface contribution of substoichiometric bonded Si-O as reported by Melinon et al. [19,20]. This hypothesis seems reasonable since we expect that our Si quantum dots will have a thin interface with the external oxide, having a substoichiometric composition with a Si-O concentration dependent on the shape of the QDs. If this is the case, the characteristics of the most shifted component in these double spectra should be attributed to the surface confinement of the phonons within the surface bonds.

A similar interpretation can be ascribed to substoichiometric boundary agglomerates between the Si nanocrystals. This point was corroborated by the infrared spectroscopy observation shown in Figure 6. Here, the region 1300–800 cm^{-1} shows the SiO_x ($x < 2$) substoichiometric oxide together with the SiO_2 contribution. In fact, in the Fourier Transform Infrared (FTIR) spectrum the contribution of the Si stoichiometric oxide is clearly present in the wide shoulder at 1200 cm^{-1}, and the Si-O stretching bonds in substoichiometric SiO_x ($x < 2$) are revealed by the main peak at 1075 cm^{-1} [21,22].

A further comment is merited by the relative intensity of the double peaks. The most shifted components, which belong to the smallest agglomerates, have variable relative intensity (see Fig. 5). This effect could be attributed to a higher concentration of small nanocrystalline clusters, resulting from the larger ones after the oxidation of the outer shell. Finally, we also note that the correlation between the size of the QDs and their linewidth excludes

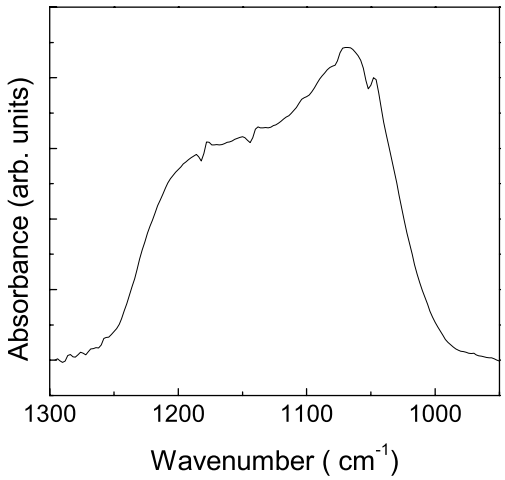

Fig. 6. Fourier transform infrared spectrum displaying the absorbance of our samples in the range typical of Si substoichiometric and stoichiometric oxides. Clearly visible is the feature around 1200 cm^{-1} due to SiO_2, and streching Si-O modes under the main peak.

any presence of amorphous agglomerates; these, in fact, should present a much wider Raman peak than that reported in our measurements [23].

In conclusion, we have observed nanosized agglomerates of Si surrounded by a Si dioxide matrix. Whenever the surrounding oxide shell is not stoichiometric, we detect satellite peaks of 2.0–2.8 nm whose intensity is comparable with that of the larger cluster ensemble, in dependence of their surface to volume ratio, concentration and spread. Alternative interpretations need further investigation.

The authors gratefully acknowledge Dr. C. Spinella and Dr. V. Raineri for TEM and AFM analyses.

References

1. G. Ledoux, O. Guillois, D. Porterat, C. Reynaud, F. Huisken, B. Kohn, V. Paillard, Phys. Rev. B **62**, 15942 (2000); M.V. Wolkin, J. Jorne, P.M. Fauchet, G. Allan, C. Delerue, Phys. Rev. Lett. **82**, 197 (1999)
2. M. Ehbrecht, H. Ferkel, F. Huisken, L. Holz, Yu. N. Polivanov, V.V. Smirnov, O.M. Steimakh, R. Schmidt, J. Appl. Phys. **78**, 5302 (1995)
3. M. Ehbrecht, B. Kohn, F. Huisken, M.A. Laguna, V. Paillard, Phys. Rev. B **56**, 6958 (1997)
4. V. Paillard, P. Puech, M.A. Laguna, R. Carles, B. Kohn, F. Huisken, J. Appl. Phys. **86**, 1921 (1999)
5. L. Ravagnan, F. Siviero, C. Lenardi, P. Piseri, E. Barborini, P. Milani, C.S. Casari, A. Li Bassi, C.E. Bottani, Phys. Rev. Lett. **89**, 285506 (2002)
6. Hua Xia, Y.L. He, L.C. Wang, W. Zhang, X.N. Liu, X.K. Zhang, D. Fang, H.E. Jackson, J. Appl. Phys. **78**, 6705 (1995)
7. Wei Cheng, Shang-Fen Ren, Phys. Rev. B **65**, 205305 (2002)
8. Jian Zi, Kaiming Zhang, Xide Xie, Phys. Rev. B **55**, 9263 (1997)
9. M. Perego, S. Ferrari, M. Fanciulli, G. Ben Assayag, C. Bonafos, M. Carrada, A. Claverie, J. Appl. Phys. **95**, 257 (2004)
10. N. Daldosso, M. Luppi, S. Ossicini, E. Degoli, R. Magri, G. Dalba, P. Fornasini, F. Rocca, L. Pavesi, S. Boninelli, F. Priolo, C. Spinella, F. Iacona, Phys. Rev. B **68**, 85327 (2003)
11. E. Magnano, C. Cepek, M. Sancrotti, F. Siviero, S. Vinati, C. Lenardi, P. Piseri, E. Barborini, P. Milani, Phys. Rev. B **67**, 125414 (2003)
12. H. Richter, Z.P. Wang, L. Ley, Solid State Commun. **39**, 625 (1981)
13. A.R. Pennisi, P. Russo, S. Gibilisco, G. Compagnini, S. Battiato, R. Puglisi, S. La Rosa, G. Faraci, *Conference Proc.* **84**, p. 183, Progress in Condensed Matter Physics, edited by G. Mondio, L. Silipigni, SIF Bologna 2003, Italy
14. Y. Guyot, B. Champagnon, M. Boudeulle, P. Mélinon, B. Prével, V. Dupuis, A. Perez, Thin Solid Films **297**, 188 (1997)
15. Wei Cheng, Shang-Fen Ren, Phys. Rev. B **65**, 205305 (2002)
16. Z. Igbal, S. Veprek, A.P. Webb, P. Capezzuto, Solid State Commun. **37**, 993 (1981)
17. Minoru Fujii, Yoshihiko Kanzawa, Shinji Hayashi, Keiichi Yamamoto, Phys. Rev. B **54**, R8373 (1996)
18. H.H. Andersen, J. Bohr, A. Johansen, E. Johnson, L. Sarholt-Kristensen, V. Surganov, Phys. Rev. Lett. **59**, 1589 (1987)
19. P. Melinon, P. Kéghelian, B. Prével, V. Dupuis, A. Perez, B. Champagnon, Y. Guyot, M. Pellarin, J. Lerné, M. Broyer, J.L. Rousset, P. Delichére, J. Chem. Phys. **108**, 4607 (1998)
20. P. Melinon, P. Kéghelian, B. Prével, A. Perez, J. Lerné, M. Pellarin, M. Broyer, J. Chem. Phys. **107**, 10278 (1997)
21. L. Ling, S. Kuwabara, T. Abe, F. Shimura, J. Appl. Phys. **73**, 3018 (1993)
22. B.J. Hinds, F. Wang, D.M. Wolfe, C.L. Hinkle, G. Lukovsky, J. Vac. Sci. Technol. **16**, 2171 (1998)
23. Takafumi Seto, Takaaki Orii, Makoto Hirasawa, Nobuhiro Aya, Thin Solid Films **437**, 230 (2003)